do not exhibit these crystal forms; only spherules of opal-CT are found. This suggests that this particular core segment did not experience any pervasive thermal anomalies which could account for these minerals. The sample was recovered from a depth of 295 m below the sea floor. Under a normal geothermal gradient, it could not have formed at temperatures significantly above 20°C; however, high cristobalite and high tridymite are thermodynamically stable above 1470° and 870°C, respectively. Furthermore, the assemblage opal-CT consisting of two varieties of quartz, cristobalite, and tridymite is highly unusual. It further illustrates the disequilibrium conditions under which this sample was formed.

The existence of discrete crystalline growths of cristobalite and tridymite in void fillings undoubtedly represents a higher degree of ordering of silica phases than the disordered cristobalite-tridymite spherules that are so common in Tertiary deep-sea cherts. Euhedral crystals found in vugs are normally assumed to represent direct precipitates. This is observed here, an indication that these crystals are direct precipitates from interstitial solutions rather than a recrystallization of former opal or cristobalite spherules. It is likely that these crystals reflect slower rates of nucleation rather than a step in the inversion from cherts rich in opal-CT to quartzose cherts.

JOHN A. KLASIK

Department of Geology,
Louisiana State University,
Baton Rouge 70803

References and Notes

1. S. E. Calvert, *Contrib. Mineral. Petrol.* **33**, 273 (1971); W. H. Berger and U. Von Rad, in *Initial Reports of the Deep Sea Drilling Project* (Government Printing Office, Washington, D.C., 1973), vol. 14, p. 787; R. Greenwood, *J. Sediment. Petrol.* **43**, 700 (1973).
2. S. W. Wise, Jr., B. F. Buie, F. M. Weaver, *Eclogae Geol. Helv.* **65**, 157 (1972); F. M. Weaver and S. W. Wise, Jr., *Trans. Gulf Coast Assoc. Geol. Soc.* **22**, 222 (1972); S. W. Wise, Jr., and F. M. Weaver, *ibid.* **23**, 305 (1973).
3. F. M. Weaver and S. W. Wise, Jr., *Nat. Phys. Sci.* **237**, 56 (1972).
4. B. Mason and L. G. Berry, *Elements of Mineralogy* (Freeman, San Francisco, 1968), pp. 516–539 and 414–415.
5. J. D. Dana (revised by C. Frondel), *The System of Mineralogy: Silica Minerals* (Wiley, New York, ed. 7, 1962), vol. 3, pp. 259–286.
6. W. A. Deer, R. A. Howie, J. Zussman, *An Introduction to the Rock-Forming Minerals* (Wiley, New York, 1966), pp. 340–355.
7. J. W. Grieg, H. E. Merwin, E. S. Sheperd, *Am. J. Sci.* **241**, 61 (1933).
8. C. E. Dutton, *Am. Mineral.* **22**, 804 (1937).
9. J. H. Oehler, *Nat. Phys. Sci.* **241**, 64 (1973).
10. C. Frondel, personal communication.
11. I thank Drs. L. P. Knauth, R. E. Ferrell, and C. Frondel for critically reading this manuscript. This research was funded by grant 1837-74 from the Geological Society of America. Samples were supplied by the JOIDES deep-sea drilling project.

19 March 1975

Internal Waves: Measurements of the Two-Dimensional Spectrum in Vertical-Horizontal Wave Number Space

Abstract. *Thermistor chain measurements of internal wave motions below the thermocline in the western North Atlantic have been spectrally decomposed in vertical-horizontal wave number space. The measured two-dimensional spectrum exhibits a systematic deviation from the corresponding Garrett and Munk model for internal wave spectra.*

Internal gravity waves are local oscillations about the equilibrium stable density stratification of the earth's oceans and atmosphere. In the ocean, the statistical properties of motions with horizontal scales ranging from tens of meters to tens of kilometers and temporal scales ranging from tens of minutes to tens of hours appear to scale consistently with the predictions of linear internal gravity wave propagation theory (*1*, *2*). The primary internal wave scaling relationship is that energy densities vary in direct proportion to the local Brunt-Väisälä frequency N, which is defined in the upper ocean in terms of the local vertical gradient, $d\rho/dz$, by

$$N^2 = -\frac{g}{\rho}\frac{d\rho}{dz}$$

where g is the acceleration of gravity. Furthermore, such motions are generally found to be statistically isotropic in horizontal planes (*3*, *4*). If such motions are in fact manifestations of random internal wave fields, then by virtue of the frequency–wave number dispersion relation for internal waves, a complete spectral decomposition of the wave field requires information in only two of the remaining three independent coordinate dimensions (time and vertical and horizontal space). Although it is unlikely that the field of internal wave motions constitutes a normal random process, there is evidence to the effect that it is very nearly normal (*5*), and it is well known that the spectrum of a normal random process provides a complete statistical description of the process (*6*).

Invoking elements of internal wave theory and drawing on available empirical data, Garrett and Munk (*2*) constructed a model (designated GM75) for the two-dimensional spectral decomposition of the internal wave field in the ocean, $F_\zeta(\alpha, \beta; \omega(\alpha, \beta))$. Unfortunately, the data base available to them was intrinsically one-dimensional, being composed of frequency spectra from moored current meters and wave number spectra from towed or dropped instruments, together with some limited coherences between pairs of instruments separated in space or time. Here, we present data on the two-dimensional spectral decomposition of the internal wave field in vertical-horizontal wave number space. Although one-dimensional spectra in the vertical and horizontal derived from our two-dimensional spectrum agree with published spectra that represent a portion of the data base for the GM75 model, systematic deviations from the complete (two-dimensional) model are observed in the vertical-horizontal wave number plane.

During the period 22 August to 12 September 1974, the U.S.N.S. *Lynch* was deployed in the western North Atlantic between Cape Hatteras and Bermuda. During this time measurements were made of the two-dimensional (vertical-horizontal) structure of the oceanic internal wave field. The basic measurement system consisted of a towed thermistor chain. The chain has connections for mounting 70 sensors at an average vertical spacing of 1.4 m at normal towing speeds. Here, we analyze the data from 32 thermistors located in the lower portion of the chain, where curvature effects associated with the chain profile are minimized during towing. For this portion of the chain, the average vertical spacing between thermistors was 1.27 m (*7*). Supporting environmental data were provided by salinity-temperature-depth (STD) recorder and profiling current meter casts and by parachute drogues deployed at various depths. The STD data provided estimates of the average temperature and Brunt-Väisälä frequency profiles, which are required for proper data scaling. The nominal center line tow depth was 100 m, which placed the thermistor array below the seasonal thermocline in a region where the average temperature gradient and Brunt-Väisälä frequency varied only slightly over the sampling region, so that special processing techniques (*8*) were not required for spectral decomposition in the vertical. Our analysis of the parachute drogue and current meter data indicates an absence of significant background current shear over the range of depths of interest here.

The thermistor chain measurements were made during four basic exercises (see Table 1), each consisting of a box pattern of four 8-km tow legs at a nominal speed of 3 m sec^{-1} (*9*). Data were sampled every

30 cm in the horizontal and averaged in 105-m increments. Only 64 such increments were retained for each tow leg in order that the spectral decomposition could be performed on an array of 64×32 points using efficient fast Fourier transform techniques (*10*). Assuming horizontal isotropy and internal wave scaling, the 16 tow legs yield 32 independent sample estimates of the two-dimensional spectral density $F_\zeta(\alpha_1, \beta)$ of internal wave amplitude, where α_1 is the horizontal wave number in the direction of tow and β is vertical wave number. Each sample spectrum resolves 32×16 wave number pairs in increments $\Delta\alpha_1 = 1.5 \times 10^{-4}$ cycle/m and $\Delta\beta = 2.5 \times 10^{-2}$ cycle/m up to the Nyquist wave numbers $\alpha_n = 4.8 \times 10^{-3}$ cycle/m and $\beta_n = 4.0 \times 10^{-1}$ cycle/m. Because the spectral estimates are obtained by direct Fourier transformation of the data grid, the sample spectra are in fact smoothed by a Bartlett window (*11*, pp. 239–243). By averaging over the 32 sample spectra, the variance of our resultant smoothed spectral estimator of $F_\zeta(\alpha_1, \beta)$ should be reduced to roughly 2 percent of the variance found in the original sample spectra (*11*, p. 252). Note that the range of wave numbers resolved by our array ($1.5 \times 10^{-4} < \alpha < 4.8 \times 10^{-3}$ cycle/m and $2.5 \times 10^{-2} < \beta < 4.0 \times 10^{-1}$ cycle/m) is well suited for internal wave analysis. It is probable that for the environmental conditions under which our data were taken, pure internal wave motions are restricted to horizontal and vertical wave numbers less than 7.5×10^{-3} and 1 cycle/m, respectively (*12*). At the other extreme, we note that the low wave number resolution of our array corresponds roughly to the low wave number resolution of previous one-dimensional studies of internal wave motions (*3*, *13*, *14*).

The data base Garrett and Munk were able to draw on in constructing their model for the internal wave spectrum was inherently one-dimensional. The one-dimensional horizontal and vertical wave number spectra $F_\zeta(\alpha_1)$ and $F_\zeta(\beta)$ are the result of collapsing the two-dimensional spectrum $F_\zeta(\alpha_1, \beta)$ onto the respective wave number axes

$$F_\zeta(\alpha_1) = \int_0^\infty F_\zeta(\alpha_1, \beta) d\beta$$

$$F_\zeta(\beta) = \int_0^\infty F_\zeta(\alpha_1, \beta) d\alpha_1$$

In Fig. 1 we have plotted the one-dimensional spectra $F_\zeta(\alpha_1)$ and $F_\zeta(\beta)$ based on the thermistor chain data. The spectra are properly normalized by the Brunt-Väisälä frequency for direct comparison with the

Table 1. Cruise data.

Exercise	Date	Location	Depth (m)	N (cycle/hour)	dT/dz (°C/m)
1	25 August 1974	34°40′N, 72°20′W	100	5.4	0.018
2	29 August 1974	31°53′N, 64°45′W	100	5.0	0.031
3	1 September 1974	31°50′N, 64°52′W	82	6.0	0.044
4	7 September 1974	34°28′N. 72°55′W	116	6.0	0.044

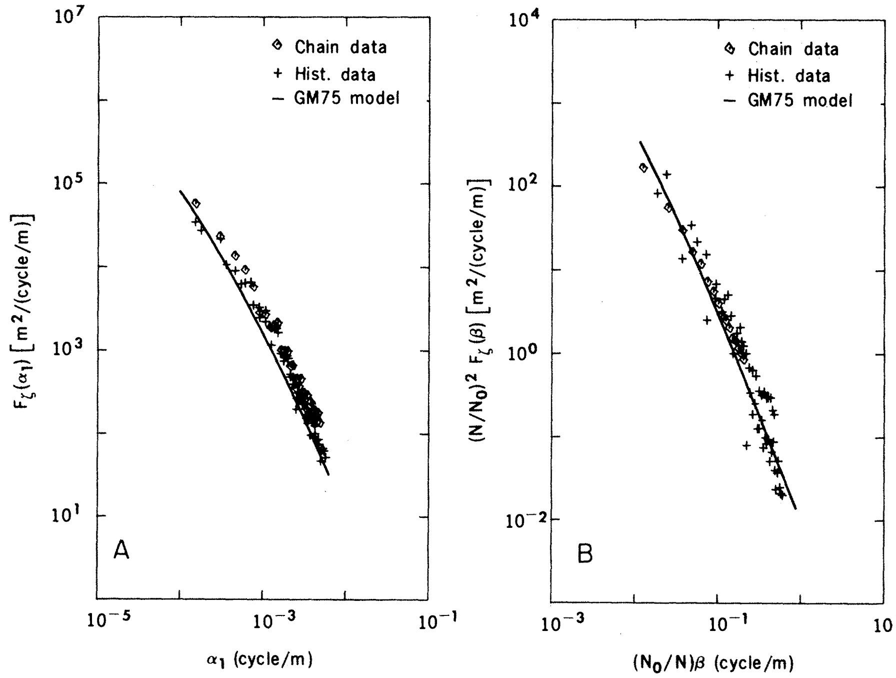

Fig. 1. Normalized horizontal (A) and vertical (B) one-dimensional spectra of internal wave amplitude.

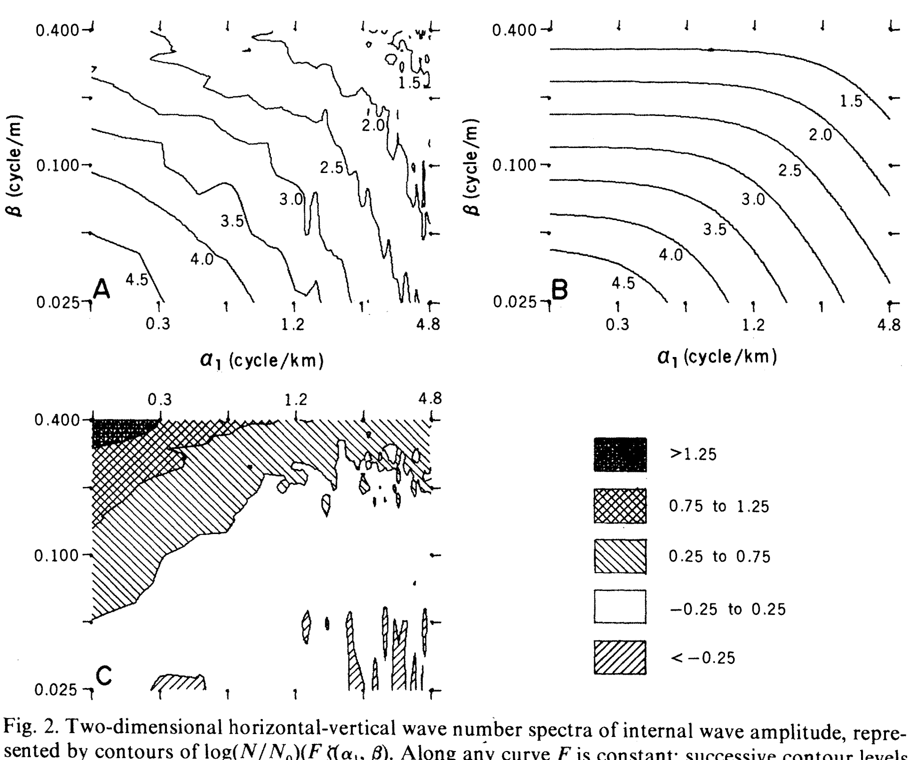

Fig. 2. Two-dimensional horizontal-vertical wave number spectra of internal wave amplitude, represented by contours of $\log(N/N_0)(F_\zeta(\alpha_1, \beta)$. Along any curve F is constant; successive contour levels are separated by 5-db increments in spectral density. (A) Measured spectrum; (B) GM75 model spectrum; (C) contours of the logarithm of the ratio of the measured to the model spectrum—that is, the difference between A and B.

GM75 model. The vertical wave number spectral estimates have been compensated for aliasing (*11*, pp. 52–53), assuming an asymptotic $\beta^{-2.5}$ dependence consistent with the GM75 model. Because the data are averaged horizontally over scales smaller than the sampling interval, the horizontal spectrum is not aliased. Also plotted in Fig. 1 are normalized one-dimensional spectral estimates drawn from several published sources (*3, 13, 14*), together with the appropriate predictions of the GM75 model. Clearly, our data are consistent with the historical data, and the GM75 model gives a fair representation of the one-dimensional spectra.

Our empirical two-dimensional spectrum is presented in Fig. 2A. Since there are no data relating to the correct asymptotic form of the two-dimensional spectrum, no attempt has been made to compensate for aliasing in the vertical. The presentation is in the form of a contour map. The wave number axes are logarithmic, and the data are represented by computer-generated contours of $\log(N/N_0)F_\xi(\alpha_1, \beta)$, the units of F being (meters)^2 (cycles per meter)$^{-2}$. Along any curve (contour) $F_\xi(\alpha_1, \beta)$ is constant, and successive contour levels are separated by 5-db increments in F. Small-scale vacillations in the contours are the result of statistical variability related to the finiteness of our data sample. The spectrum is roughly symmetric about the line $\beta = \alpha_1 N/f$, which corresponds to a (45°) diagonal passing through the point (α_1, β) = (0.2 cycle/km, 0.025 cycle/m).

This behavior is consistent with the results of a scale analysis of the internal wave equation, which indicate that vertical and horizontal dimensions in the internal wave field should scale roughly in the ratio f/N, where f is the local inertial frequency (2 cycles per day times the sine of the latitude). The corresponding GM75 model spectrum is plotted in Fig. 2B, and although the model gives a fair representation of the data for $\beta \lesssim \alpha_1 N/f$, it exhibits a trend of systematic deviation from the data for $\beta \gtrsim \alpha_1 N/f$. This trend is emphasized in Fig. 2C, where we have contoured the logarithm of the ratio of the empirical spectral density to the model spectral density—that is, the difference between A and B of Fig. 2. The effect of aliasing on the measured spectrum should be confined to a narrow band along the top of Fig. 2C, the maximum effect being a 3-db (0.3 unit of $\log F$) rise in the spectrum at $\beta = 0.4$ cycle/m. Taking into account the vertical aliasing, it would appear that the deviation is primarily a function of the ratio α_1/β. Since the frequency–wave number dispersion relation takes the form

$$\omega^2 = f^2(1 + \alpha^2 N^2/\beta^2 f^2)$$

for waves with frequency $\omega \ll N$, this implies that the deviation is primarily a function of frequency, rather than wave number per se. That is, the GM75 model systematically underestimates the measured spectrum as ω tends down to the inertial frequency. Note that this systematic deviation is much less apparent in the integrated or one-dimensional spectra, although a close examination of Fig. 1 indicates that the GM75 model does not precisely predict the data. Unfortunately, conversion of the α_1-β spectra to a frequency spectrum via the dispersion relation greatly amplifies the statistical "noise" in the experimental data since the derivative $\delta F/\delta\alpha_1$ is required in order to estimate $F(\alpha,\beta;\omega(\alpha,\beta))$, so that a meaningful quantitative comparison of our data with historical data from moored sensors is virtually impossible. However, we do note that the nature of the deviation between GM75 and our data appears at least to be consistent with the fact that although simple wave theory (as incorporated in the GM75 model) dictates that inertial period motions produce no sensible vertical displacements, vertical displacements are indeed found to be associated with inertial period motions in the sea (*15*).

T. H. Bell, Jr., J. M. Bergin
J. P. Dugan, Z. C. B. Hamilton
W. D. Morris, B. S. Okawa, E. E. Rudd
Ocean Sciences Division, Naval Research Laboratory, Washington, D.C. 20375

References and Notes

1. N. P. Fofonoff and F. Webster, *Philos. Trans. R. Soc. Lond. Ser. A Math. Phys. Sci.* **270**, 349 (19 W. J. Gould, *ibid.*, p. 437.
2. C. Garrett and W. Munk, *Geophys. Fluid Dyn.* **3**, 225 (1972); *J. Geophys. Res.* **80**, 291 (1975).
3. E. J. Katz, *J. Phys. Oceanogr.* **3**, 448 (1973).
4. S. A. Kitaygorodskiy, Yu. Z. Miropol'skiy, B. N. Filyushkin, *Izv. Akad. Nauk SSSR Phys. Atmos. Okean.* **9**, 272 (1973).
5. For the data analyzed here, the skewness of the probability density function is 0.01 and the kurtosis is 3.73.
6. A. M. Yaglom, *An Introduction to the Theory of Stationary Random Functions*, translated and edited by R. A. Silverman (Prentice-Hall, Englewood Cliffs, N.J., 1962), p. 15.
7. Because of peculiarities of chain construction and towing configuration, there is a systematic variability of ± 0.24 m in thermistor spacing. However, numerical studies indicate that this variability has little effect on our spectral decomposition, and we treat the data as if they were uniformly spaced in the vertical.
8. T. H. Bell, *J. Phys. Oceanogr.* **4**, 669 (1974).
9. Using the frequency–wave number dispersion relation for internal waves, it is readily established that the average internal wave phase speed in the direction of tow for each vertical-horizontal wave number pair resolved by our array is small compared to the tow speed, and we are thereby justified in replacing elapsed time by horizontal distance in our analysis of the data.
10. The total deviation from the vertical of the active portion of the chain considered here was less than the 105-m averaging interval, so that for purposes of analysis the 64 × 32 point data grids represent matrices of uniformly spaced smooth temperatures. See also (*7*).
11. G. M. Jenkins and D. G. Watts, *Spectral Analysis and Its Applications* (Holden-Day, San Francisco, 1968).
12. T. H. Bell, *Geophys. Res. Lett.* **1**, 253 (1974); R. S. McKean and T. E. Ewart, *J. Phys. Oceanogr.* **4**, 191 (1974).
13. A. D. Voorhis and H. T. Perkins, *Deep-Sea Res.* **13**, 641 (1966).
14. N. G. Garnich, Yu. Z. Miropol'skiy, V. I. Prokhorov, K. N. Federov, *Izv. Akad. Nauk SSSR Phys. Atmos. Okean.* **9**, 155 (1973); S. P. Hayes, T. M. Joyce, R. C. Millard, *J. Geophys. Res.* **80**, 314 (1975).
15. C. Rooth and W. Duing, *J. Phys. Oceanogr.* **1**, 12 (1971).

20 February 1975; revised 9 April 1975

Leukocyte Recruitment to Airways by Cigarette Smoke and Particle Phase in Contrast to Cytotoxicity of Vapor

Abstract. *After hamsters had breathed fresh cigarette smoke in a miniature chamber, airways of the lung showed recruitment of polymorphonuclear leukocytes. Exposure to particles alone by removal of the vapor phase with charcoal did not change the leukocyte response. However, exposure to cigarette smoke vapor after removal of particles with Cambridge filters did not recruit leukocytes but produced nuclear and cytoplasmic vacuoles, double nuclei, and exfoliation of cells.*

Cigarette smoking over a long period is associated with cough, sputum production, and chronic bronchitis in many human subjects (*1*). The mechanism of the bronchitis is unclear. Cigarette smoking and exposure to other airborne agents such as cotton dust are additive in producing chronic bronchitis, as found in cotton textile workers (*2*). Exposure to cotton dust recruited polymorphonuclear leukocytes to nasal airways in human subjects (*3*) and in pulmonary airways of rodents (*4*). The link between cotton dust exposure and cigarette smoking suggested that smoking may recruit leukocytes to airways. The immediate effects of cigarette smoking include reduced early phase of particle clearance (*5*), increased closing volume (*6*), increased airway resistance (*7*), and toxic effects on oral leukocytes (*8*). We now report that in hamsters inhaled cigarette smoke recruits polymorphonuclear (PMN) leukocytes to airway lumens from trachea to terminal bronchioles. The particle phase of the smoke has the same effect. However, the vapor phase alone is cytotoxic to epithelial cells, especially the nonciliated ones.

Hamsters were used to study the immediate effects of airborne exposure to unfiltered whole cigarette smoke, vapor phase alone, and particle phase alone. A novel